Excitation Density Dependent Photoluminescence Quenching and Charge Transfer Efficiencies in Hybrid Perovskite/Organic Semiconductor Bilayers

Jinhyun Kim, Robert Godin, Stoichko D. Dimitrov, Tian Du, Daniel T. J. Bryant, Martyn A. McLachlan, and James R. Durrant*

This study addresses the dependence of charge transfer efficiency between bilayers of methylammonium lead iodide ($MAPI_3$) with $PC_{61}BM$ or poly(3,4-ethylenedioxythiophene): polystyrene sulfonate (PEDOT:PSS) charge transfer layers on excitation intensity. It analyzes the kinetic competition between interfacial electron/hole transfer and charge trapping and recombination within $MAPI_3$ by employing a range of optical measurements including steady-state (SS) photoluminescence quenching (PLQ), and transient photoluminescence and absorption over a broad range of excitation densities. The results indicate that PLQ measurements with a typical photoluminescence spectrometer can yield significantly different transfer efficiencies to those measured under 1 Sun irradiation. Steady-state and pulsed measurements indicate low transfer efficiencies at low excitation conditions (<5E + 15 cm^{-3}) due to rapid charge trapping and low transfer efficiencies at high excitation conditions (>5E + 17 cm^{-3}) due to fast bimolecular recombination. Efficient transfer to $PC_{61}BM$ or PEDOT:PSS is only observed under intermediate excitation conditions (≈1 Sun irradiation) where electron and hole transfer times are determined to be 36 and 11 ns, respectively. The results are discussed in terms of their relevance to the excitation density dependence of device photocurrent generation, impact of charge trapping on this dependence, and appropriate methodologies to determine charge transfer efficiencies relevant to device performance.

1. Introduction

Photovoltaic cells based on solution processed, organolead halide perovskite materials have surpassed 20% solar energy conversion efficiencies, and are attracting increasing interest for commercial applications.[1] Such materials exhibit a range of favorable optoelectronic properties for photovoltaic device function, including large absorption coefficients for light absorption and high charge carrier mobilities to enable rapid charge transfer from the photoactive layer.[2] A key consideration determining the efficiency of such devices is the kinetic competition between the extraction of photogenerated charges from the photoactive perovskite layer to the external circuit versus charge recombination and trapping processes within this layer and at its interfaces. This kinetic competition, which determines transfer efficiency, is strongly dependent on film processing and device architecture, and also dependent on light irradiation intensity and device operating condition (e.g., short circuit vs maximum power point). In particular, whilst several studies have reported a strong, and complex, dependence of charge carrier recombination and trapping processes upon light intensity in methylammonium lead iodide ($MAPI_3$) films,[3] studies of the impact of this light intensity dependence upon the kinetics and efficiency of charge transfer from the $MAPI_3$ layer to electron and hole transfer layers have been limited to date.[4] This dependence is not only important to understand the irradiation intensity dependence of device efficiency but also critical in determining the relevance of steady-state (SS) and pulsed assays of these transfer processes to device operation. Such assays are often undertaken under irradiation conditions very different from steady-state solar irradiation, a consideration which has received little attention to date in studies of the impact of these charge transfer processes upon device performance. In the study herein, we therefore investigate the light intensity dependence of these charge transfer processes employing a range of both steady-state and transient optical measurements, and discuss the relevance of these studies to the efficiency of photocurrent generation under solar irradiation.

J. Kim, R. Godin, T. Du, D. T. J. Bryant, J. R. Durrant
Department of Chemistry
Centre for Plastic Electronics
Imperial College London
London SW7 2AZ, UK
E-mail: j.durrant@imperial.ac.uk
S. D. Dimitrov, J. R. Durrant
SPECIFIC
College of Engineering
Swansea University
Bay Campus, Swansea SA1 8EN, UK
T. Du, M. A. McLachlan
Department of Materials
Centre for Plastic Electronics
Imperial College London
London SW7 2BP, UK
The ORCID identification number(s) for the author(s) of this article can be found under https://doi.org/10.1002/aenm.201802474.

DOI: 10.1002/aenm.201802474

Photoluminescence (PL) spectroscopy is the most widely used technique to study excited state dynamics in hybrid perovskite films and devices. Such studies include the determination of charge carrier diffusion lengths and transfer yields in the presence of electron/hole charge transfer layers, and in complete devices.[2b,5] In particular the measurement of steady-state PL quenching efficiency (PLQE) has been used in many of the pioneering works on perovskite photovoltaics to assess the relationship between interfacial charge transfer, charge extraction, and device performance.[5j,6] In such studies the PLQE is calculated from the ratio of the PL emission intensity of the perovskite layer with and without the quencher interlayers, where the loss of PL is interpreted as a marker of charge transfer. Such PLQE measurements have indicated hole transfer efficiencies for many perovskite materials higher than 95% for a broad range of p-type materials used as hole extracting layers in cells, including NiO, Spiro-OMeTAD, poly(3,4-ethylenedioxythiophene): polystyrene sulfonate (PEDOT:PSS), and V_2O_5. Similarly, the PLQE measurements with n-type contacts such as PFN and $PC_{61}BM$ have also been found to be very high, often >98%,[7] indicative of near unity electron transfer efficiencies. However, despite PLQE measurements indicating near unity electron and hole transfer efficiencies, the resulting device photocurrents have often shown wide variations. This may in part result from contact layer selectivity, with for example PEDOT:PSS having the potential to accept both holes and electrons from $MAPI_3$, thereby potentially resulting, in the absence of appropriate electric fields, in enhanced surface recombination losses.[8] In addition, almost all such PLQE studies have been undertaken in standard PL spectrometers, where the irradiation intensity is typically of the order of a few mW cm^{-2}, one to two orders of magnitude lower than solar irradiation. This key consideration has not been taken into account in most such studies. More limited studies have reported a strong excitation intensity dependence of PL intensity and quenching yields in $MAPI_3$ films in the presence of charge transfer layers, although the relevance of this to the kinetics and efficiency of interfacial charge transfer and its impact on device performance remains unclear.[9] Several studies have also reported that the PL intensity of the $MAPI_3$ films alone is strongly dependent not only upon film processing but also may evolve following deposition depending upon storage conditions (light exposure, temperature, environment, etc.), further complicating the use of photoluminescence measurements as an assay of charge transfer efficiency.[10] As such, it is apparent that employing conventional PLQE spectrometer measurements may not be a reliable tool to assay the efficiency of charge transfer processes in $MAPI_3$ devices operating under 1 Sun irradiation.

In addition to PL quenching measurements, transient photoluminescence, absorption, and microwave conductivity measurements have been used to study the kinetics and yields of charge transfer from between the $MAPI_3$ layer and electron/hole transfer layers.[4d,11] Such studies have been conducted with widely varying light excitation densities.[12] Typically, transient PL measurements are conducted using time-correlated single photon counting (TCSPC) spectrometers, which employ very low energy pulsed irradiation (usually ≈10 pJ cm^{-2} per pulse) but at relatively high repetition rates (MHz), whilst transient absorption measurements are undertaken at much higher pulse energies (usually 1–10 μJ cm^{-2}) and lower repetition rates (kHz). Both of these irradiation conditions are significantly different from steady-state solar irradiation, complicating considerations of the relevance of the data obtained to device operation.

In the study herein, we investigate the impact of excitation density dependence on the steady-state and transient photoluminescence and transient absorption properties of $MAPI_3$ thin films and $MAPI_3/PC_{61}BM$ and PEDOT:PSS/$MAPI_3$ bilayers. $PC_{61}BM$ and PEDOT:PSS correspond to two widely employed electron and hole transfer layers.[9b,13] We note that whilst $PC_{61}BM$'s energy level alignment results in it being a selective contact layer for electron transfer from $MAPI_3$, the high doping of PEDOT:PSS results it being potentially able to accept both electrons and holes from $MAPI_3$, as discussed above. For simplicity, and consistent with its function in perovskite devices, we will assume herein its functions as primarily as a hole transfer layer; a point we return to in the discussion below. Four different experimental techniques were applied to investigate the dynamics of charge transfer as a function of excitation intensity, namely femtosecond time resolution transient absorption spectroscopy (fs-TAS), steady-state PL (ss-PL) spectroscopy and two pulsed PL measurements operating under very different excitation density ranges: TCSPC under high repetition rate, low pulse energy excitation conditions, and nanosecond time resolution PL measurements operating under low repetition rate, high pulse energy excitation conditions more comparable to those employed in fs-TAS measurements (ns-PL). These techniques allow us to probe the efficiency and kinetics of charge transfer over a broad range of excitation conditions, generating carrier densities in the $MAPI_3$ film ranging from 10^{12} to 10^{18} cm^{-3}. The results from these studies allow us to elucidate how charge density-dependent monomolecular and bimolecular recombination in the $MAPI_3$ film competes with charge transfer under different excitation densities, with important implications for the light intensity dependence of device operation and the identification of suitable experimental protocols to assay these transfer processes under conditions relevant to such device operation.

2. Results

For this study, $MAPI_3$ perovskite films were prepared by the toluene antisolvent dripping method with γ-butyrolactone (GBL) and dimethyl sulfoxide (DMSO) precursor solvents, as detailed previously.[14] This is an established fabrication methodology known to produce dense and highly crystalline $MAPI_3$ films reasonably reproducibly.[15] The "inverted" device structure of Glass/indium tin oxide (ITO)/PEDOT:PSS/$MAPI_3/PC_{61}BM$/LiF/Al was fabricated to test the quality of the films studied and their relevance to published work (following film storage in the glove box as discussed below). Such devices had *J–V* curves typical of those reported for this structure (Figure S1, Supporting Information), with power conversion efficiencies in the range 13–16%.[7,16] For spectroscopic studies of electron and hole transfer, three film structures were prepared following the same procedures as for device preparation: $MAPI_3$ (≈290 nm thick), $MAPI_3/PC_{61}BM$, and PEDOT:PSS/$MAPI_3$. The film absorption

spectra were typical of well-formed $MAPI_3$ crystals, as seen from the SEM images in Figures S2 and S3 in the Supporting Information. Consistent with previous reports,[14a] the photoluminescence (PL) intensity of $MAPI_3$ films was observed to evolve significantly following film fabrication, even for films stored in the dark in a glove box, showing an increase in intensity over a 10 d period before stabilizing (Figure S4, Supporting Information). As such, we controlled for the evolution of the PL behavior by performing all measurements on samples kept in the dark in a glove box for 12 d prior to measurement. We note that after this storage treatment, film PL intensity was relatively insensitive to light soaking, thereby simplifying data analysis (Figure S5, Supporting Information).

Figure 1a shows the conventional SS-PL spectra of $MAPI_3$, $MAPI_3/PC_{61}BM$, and PEDOT:PSS/$MAPI_3$ films recorded with 635 nm excitation at a light fluence of 1.5 mW cm^{-2}, corresponding to typical fluorimeter excitation conditions. This excitation is much lower than the photon fluence under 1 Sun AM 1.5 conditions (≈1.8% of 1 Sun). The neat $MAPI_3$ (blue line) film shows typical strong emission with a maximum at ≈765 nm, as expected for this material.[11a,17] The photoluminescence from $MAPI_3$ in the $MAPI_3/PC_{61}BM$ (red dash line) and PEDOT:PSS/$MAPI_3$ (purple dot line) films is strongly quenched by the presence of the interlayers. This quenching efficiency was quantified using the equation $PLQE(\%) = (I_0 - I/I_0) \times 100$, where I_0 is the neat $MAPI_3$ film peak intensity of the emission and I is the peak intensity of the emission from the bilayers. The PLQE obtained for $MAPI_3/PC_{61}BM$ is 91% and for PEDOT:PSS/$MAPI_3$ it is 97%. Following the fabrication and storage procedure detailed above, this PLQE measurement was found to be reproducible within ±2% and insensitive to light presoaking. These PLQE data are consistent with the values reported in the literature.[7,9a,11c] However and indicate reasonably efficient transfer of electrons and holes from $MAPI_3$ to $PC_{61}BM$ and PEDOT:PSS respectively under this irradiation condition.

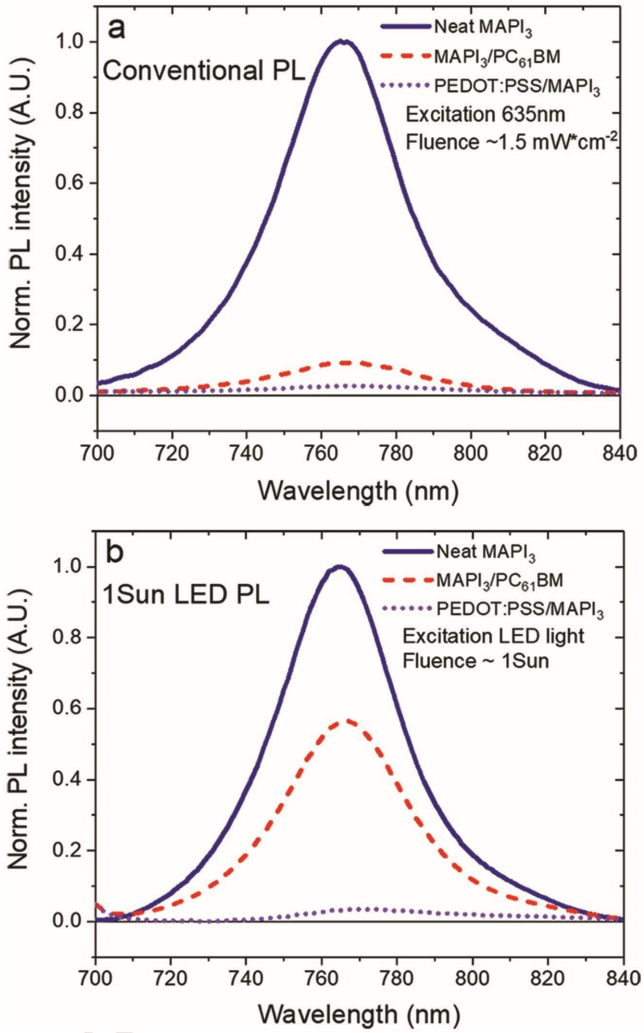

Figure 1. a) Steady-state PL (SS-PL) spectra of $MAPI_3$ (blue line), $MAPI_3/PC_{61}BM$ (red dashed line), and PEDOT:PSS/$MAPI_3$ (purple dotted line) films collected in a conventional PL spectrometer with 635 nm excitation at a light fluence of 1.5 mW cm^{-2}. b) Equivalent PL spectra of the same films collected using a white light LED excitation source with a power output selected to be equivalent to 1 Sun fluence.

In addition to this standard method for assessment of PLQE, the PL spectra of the films were recorded using a white light LED excitation source with a power output selected to correspond to ≈1 Sun photon fluence (estimated by normalizing against current densities obtained with AM1.5 irradiation). Figure 1b presents the PL spectra of the samples, which show differing relative amplitudes from those measured with the standard spectrometer light excitation source (Figure 1a). In particular, while the PLQE of the PEDOT:PSS/$MAPI_3$ film is unchanged at 97%, the PLQE of $MAPI_3/PC_{61}BM$ is substantially lower, dropping from 91% down to 46%. This result clearly indicates the importance of light intensity when conducting PLQE measurements, particularly when considering the ability of electron transfer to compete with charge trapping and recombination within the $MAPI_3$ film.

Figure 2a (open symbols) shows the integrated PL intensities of neat $MAPI_3$, $MAPI_3/PC_{61}BM$, and PEDOT:PSS/$MAPI_3$ films plotted as a function of excitation intensity (I_{ex}) from a white light LED source with irradiation intensities equivalent to 0.0008 to 3.7 Suns. The results, plotted with double-logarithmic scales, show that for the neat $MAPI_3$ film, the PL intensity (PL_0) follows approximately $PL_0 \alpha\ I_{ex}^{\beta}$ where $\beta \approx 2$ at low intensities and ≈1 at high intensities (Figure S6, Supporting Information). Similar super-linear behavior has been reported previously[3a,18] and assigned to a transition from primarily monomolecular processes at low intensities to bimolecular processes at higher intensities, as discussed further below. Both bilayer films also showed super-linear, but more complex, dependencies of PL intensity upon excitation intensity, as analyzed further below.

The PL data shown in Figure 2a were employed to determine the light intensity dependence of the PLQE for the bilayers $MAPI_3/PC_{61}BM$ and PEDOT:PSS/$MAPI_3$, as plotted in Figure 2b (open symbols). The PLQE of $MAPI_3/PC_{61}BM$ peaks near 84% at a low fluence (0.15% of 1 Sun) and decreases to 50% at 0.93% of 1 Sun before plateauing. The PLQE decreases again for intensities above 100% of 1 Sun. The PLQE of PEDOT:PSS/$MAPI_3$ rises from an initial value of 83% and reaches 98% at about 0.5% of 1 Sun, and retains this high value until dropping slightly (by ≈1%) for excitation intensities above 100% of 1 Sun. We note that the PLQE was also observed to exhibit a modest dependence upon excitation wavelength (Figure S7,

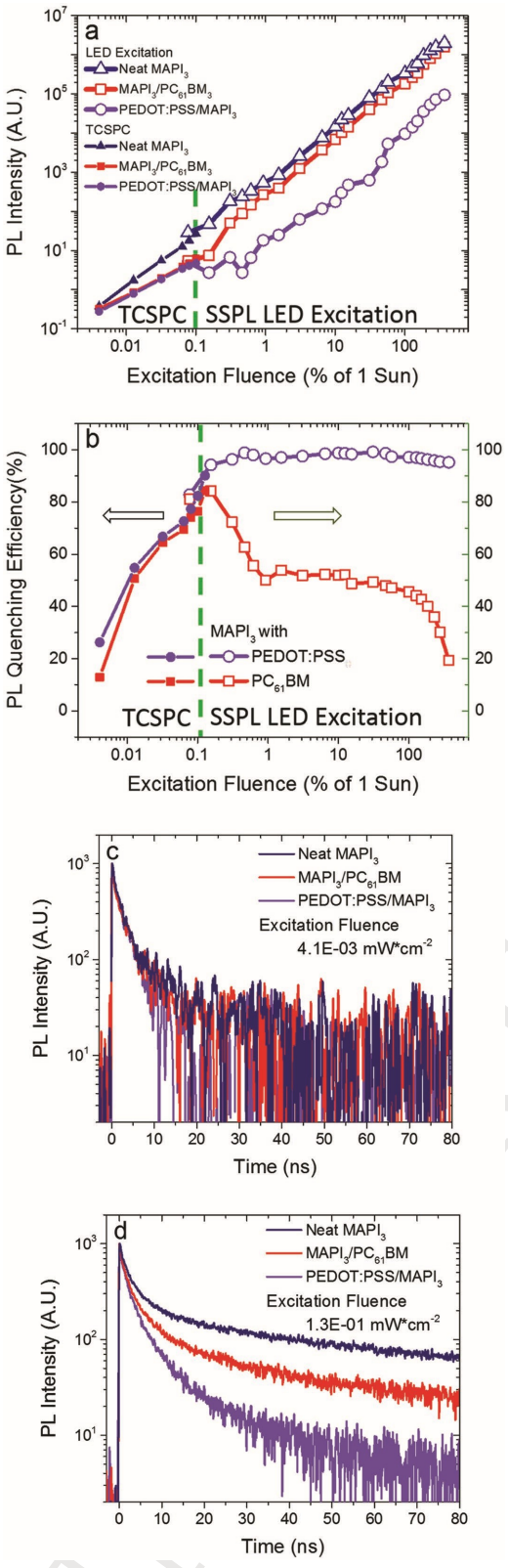

Figure 2. a) Integrated PL intensities acquired with steady-state PL spectrometer of neat $MAPI_3$ (blue triangle), $MAPI_3/PC_{61}BM$ (red square), and PEDOT:PSS/$MAPI_3$ (purple circle) films plotted on a double-logarithmic scale for excitation densities ranging from 0.08 to 370% 1 Sun equivalent. Open symbols correspond to data obtained using CW LED irradiation, whilst closed symbols correspond to integrated TCSPC decays. b) The corresponding photoluminescence quenching efficiencies are determined from these PL data. TCSPC decay dynamics of the same films measured under c) 4.1×10^{-3} mW cm^{-2} and d) 1.3×10^{-1} mW cm^{-2} excitation densities (≈0.0041% and 0.13% of 1 Sun, respectively).

Supporting Information), which explains the modest difference in PLQE's determined from the monochromatic excitation data in Figure 1 and the white light excitation in Figure 2.

We turn now to TCSPC measurements of the PL decay kinetics for the three samples studied. TSCPC is widely employed to study PL decay dynamics in $MAPI_3$ films and is typically, as based on measurements of single photons, undertaken at very low excitation fluences. For the study herein, we employed a pulse repetition rate of 1 MHz and pulse densities in the range of 5.7 to 178 pJ cm^{-2}, corresponding to quasi-CW irradiation intensities ranging from 0.004 to 0.13 mW cm^{-2}. We note that this excitation range, which is typical of TCSPC studies, is lower than the excitation densities employed for the other techniques employed in this study. TCSPC data collected at the 765 nm peak position of PL for neat $MAPI_3$ films and the two bilayers at the lowest and highest intensities are shown in Figure 2c,d; full data sets over a range of intensities for each film, and the double exponential fitting parameter and the plot as a function of excitation fluence are shown in Figure S8, Table S1, and Figure S9 in the Supporting Information, respectively. For the lowest excitation density (Figure 2c), almost identical PL decays are seen for the $MAPI_3$, $MAPI_3/PC_{61}BM$ and PEDOT:PSS/$MAPI_3$ films, with all three samples exhibiting a rapid, exponential ($\tau \approx 1.7$ ns) decay. At higher excitation densities, a slower, 10's of nanoseconds, decay phase is increasingly apparent, with this phase being largest and slowest for the $MAPI_3$ film alone (Figure 2c,d and Figure S8, Supporting Information). Following literature studies, the fast (1.7 ns) decay phase is assigned to monomolecular charge trapping, and the 10's of nanoseconds decay phase to bimolecular recombination, with the increasing dominance of this nanosecond decay phase at higher excitation intensities assigned to trap filling.[19] The observation of similar decay kinetics for all three samples at the lowest excitations conditions indicates that electron/hole transfer to $PC_{61}BM$/PEDOT:PSS is unable to compete kinetically with charge trapping at this excitation condition. It further indicates that charge trapping is not changed by the presence of the contact layers, indicating that the photoluminescence quenching observed at higher excitation conditions does not derive from increased charge trapping due to for example the generation of surface defects, but rather from charge transfer to the contact layers. At the higher excitation conditions, the 10's of nanosecond decay phase is strongly quenched by these layers, indicative of electron/hole transfer competing effectively with bimolecular recombination.[4b,9a] This behavior is further illustrated in Figure 2a,b (solid symbols), where plots of the integrated PL intensity and quenching efficiencies determined from these TCSPC data are shown to be in excellent agreement with, and extend to lower light fluxes, the data obtained with continuous irradiation. For both bilayers, the slow decay phase time constant saturates at higher excitation densities (Figure S9b, Supporting Information) with decay

time constants of 36 and 11 ns with $PC_{61}BM$ and PEDOT:PSS, respectively. These correspond to conditions of efficient electron/hole transfer, and thus indicate with transfer times of ≈36 and 11 ns for electron and hole transfer, respectively. The saturation of this decay time for both bilayers indicates that the kinetics of electron/hole transfer are relatively intensity independent, as expected for a monomolecular charge transfer process. As such, the intensity dependence of the PL decays and the PLQE data determined from these TCSPC data are assigned to the intensity dependence of competing charge trapping and bimolecular recombination processes in the $MAPI_3$ film itself.

The nonlinear PL and PLQE intensity dependencies shown in Figures 1 and 2 can be understood as resulting from variations in charge carrier density with excitation density. However, this dependence is difficult to access directly from these (quasi-) steady-state spectroscopic studies, as the accumulated charge carrier density will depend upon the carrier lifetimes, which are themselves excitation density (and transfer layer) dependent. As such we turn now to slower repetition rate pulsed laser measurements, where it is reasonable to assume no charge accumulation between laser pulses. For such measurements, the pulse energy can be directly converted into initial densities of photoinduced charge carriers, assuming that all absorbed photons generate charge carriers. For reference, we note that previous differential charge measurements on analogous devices have indicated charge carrier densities in similar $MAPI_3$ films of $\approx 10^{16}$ cm^{-3} under 1 Sun equivalent irradiation at open circuit, decreasing with lower light intensities.[20]

We consider first the low repetition rate pulsed PL measurements, employing a pulsed Nd:YAG OPO laser (5 ± 2 ns pulse width, 20 Hz) and Si-photodiode detector with a 200 ns response function. The peak PL intensity of the three samples were recorded for different excitation densities, and therefore approximate carrier densities, ranging from 9×10^{14} to 3×10^{18} cm^{-3}, as plotted in **Figure 3**a. Based on these data, the PLQE of the samples were calculated and plotted in Figure 3b. Both bilayers show a rise PLQE up to 10^{16} cm^{-3} excitation density, followed by a drop in PLQE for higher excitation densities. The dependence on excitation density is much more pronounced for $MAPI_3/PC_{61}BM$, as also observed in the steady-state PLQE data (Figure 2b). These data suggest that at carrier densities $\approx 10^{16}$ cm^{-3}, further charge trapping into nonradiative trap states is inhibited, allowing efficient charge transfer of the excess charge carriers. At higher carrier densities however the PLQE decreases with increasing excitation intensity due to speeding up band-to-band bimolecular recombination and possible Auger recombination.[21]

Finally, we turn to fs-TAS studies. TAS is another optical technique widely used for charge transfer studies in perovskite devices.[22] However, due to its lower sensitivity, it is normally conducted at much higher excitation densities than most PL techniques. The excitation densities were varied between 10^{16} and 10^{18} cm^{-3} and the photogenerated charge dynamics probed by recording the absorption change at the maximum of the negative signal at 755 nm (Figure S10, Supporting Information), typically assigned to the $MAPI_3$ ground state bleaching.[2c,23] **Figure 4**a shows typical fs-TAS absorption spectra of neat $MAPI_3$ film measured in the visible spectral range.

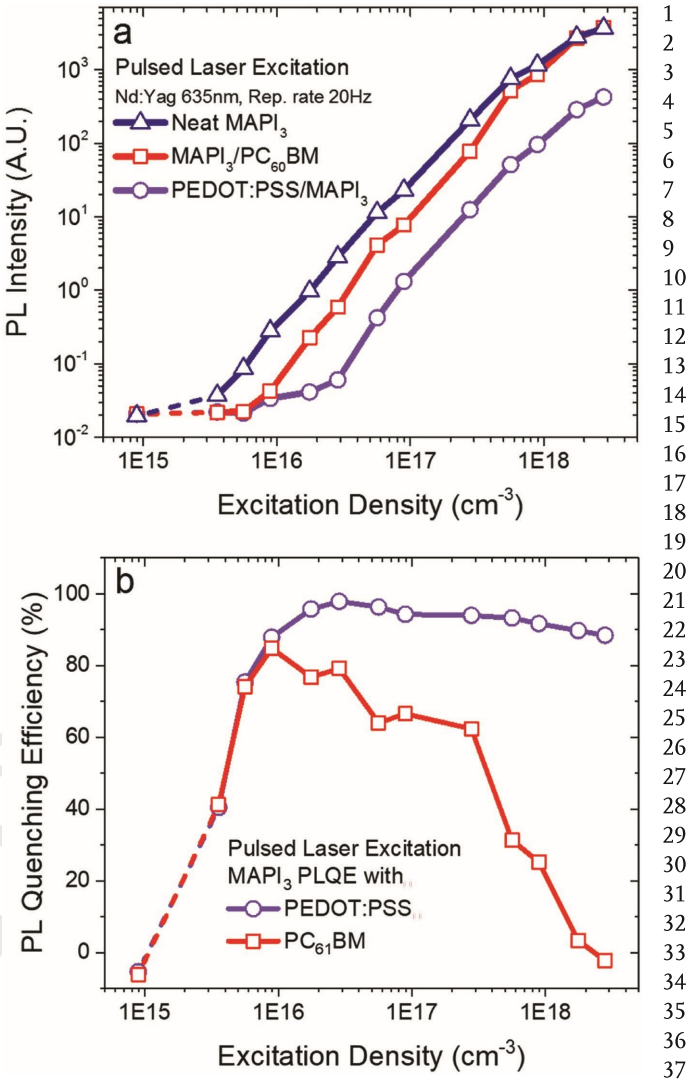

Figure 3. a) Integrated PL amplitudes of neat $MAPI_3$ (blue triangle), $MAPI_3/PC_{61}BM$ (red square), and PEDOT:PSS/$MAPI_3$ (purple circle) films determined using low repetition rate pulsed laser excitation, plotted on double-logarithmic scales for excitation densities ranging from 9×10^{14} to 3×10^{18} cm^{-3}. b) $MAPI_3$ film PLQE with $PC_{61}BM$ (red square) and PEDOT:PSS (purple circle) determined from these data as a function of excitation density.

Figure 4b plots the dynamics of the $MAPI_3$ bleach signal for time delays up to 6 ns as a function of excitation density (bilayers are in Figure S11, Supporting Information). There are two excitation density dependent decay phases apparent in these data: an initial sub-ps decay which disappears at higher excitation densities and a much slower (nanosecond) decay phase which appears only at higher excitation densities. Such data are similar to those reported previously; the sub-ps decay phase is assigned to ultrafast charge trapping/relaxation that saturates at higher laser intensities, whilst the slower decay is assigned to bimolecular charge recombination.[3c,4a,22d,23a,24] Figure 4c,d compares the bleach decay kinetics of neat $MAPI_3$ with $MAPI_3/PC_{61}BM$ and PEDOT:PSS/$MAPI_3$ bilayers at excitation densities of 3.3×10^{16} and 6.8×10^{17} cm^{-3}, respectively.

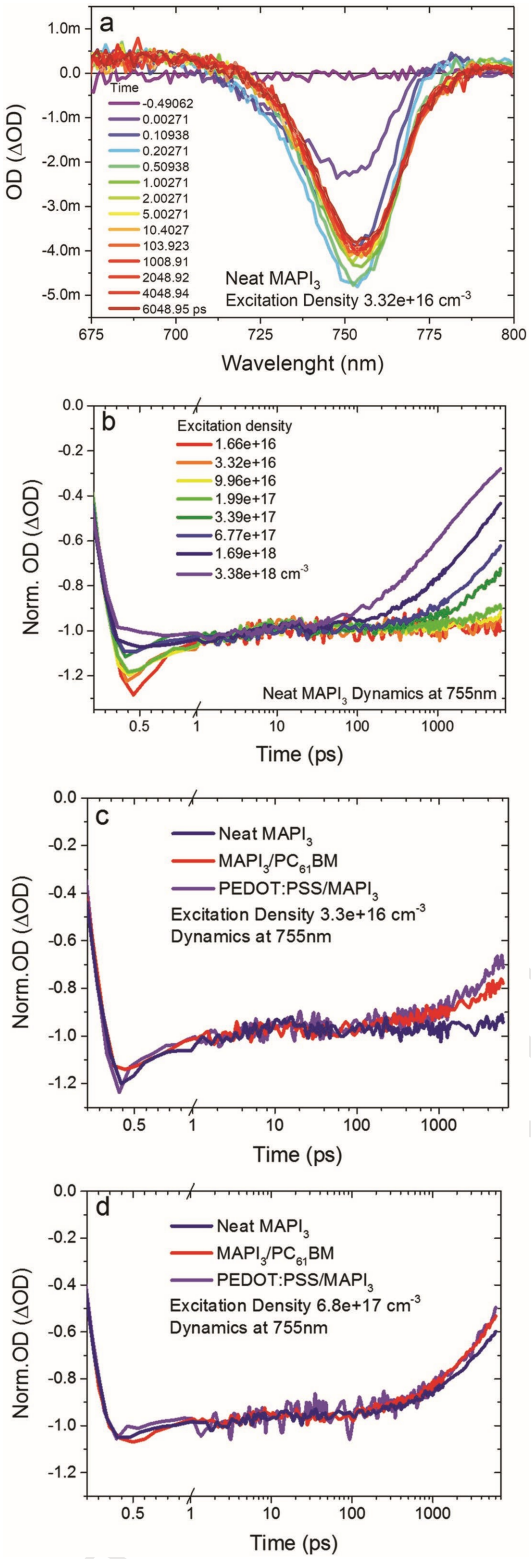

Figure 4. a) Transient absorption spectra of an $MAPI_3$ film for time delays up to 6 ns and b) the corresponding kinetics at 755 nm acquired at varied excitation densities. Comparisons of the 755 nm kinetics of neat $MAPI_3$ (blue line) with $MAPI_3/PC_{61}BM$ (red line) and PEDOT:PSS/$MAPI_3$ (purple line) at excitation densities of c) 3.32×10^{16} and d) 6.77×10^{17} cm^{-3}. Time axes are linear up to 1 ps and logarithmic for longer times.

The former excitation density corresponds to carrier densities near those in devices under 1 Sun irradiation. At this excitation density, negligible bimolecular recombination is observed for the $MAPI_3$ film alone over the timescale plotted (up to 6 ns). In contrast, both bilayers show significant nanosecond decays, which can be attributed to electron transfer to $PC_{61}BM$ and hole transfer to PEDOT:PSS. We note given the limited time range of the data, transfer times cannot be accurately estimated from these data, although they appear consistent with the 10's of nanosecond timescale determined from the TCSPC data above. For the higher excitation density, 6.8×10^{17} cm^3, the $MAPI_3$ film alone shows a significant nanosecond decay phase (decay time ≈8 ns), assigned to bimolecular recombination (we note under these conditions, excessive charge accumulation on the contact layers may also impede charge transfer). Both bilayers show only marginally faster decay kinetics than the $MAPI_3$ film alone, indicative of the 8 ns estimated bimolecular recombination time being faster than the time constants for electron/hole transfer (see Figure S12, Supporting Information, for lifetime fitting). This result is also consistent with the loss of PLQE observed at high excitation densities in Figure 3, and is indicative that under these excitation conditions, electron/hole transfer is unable to kinetically compete with rapid bimolecular charge recombination in the $MAPI_3$ film.

3. Discussion

Photoluminescence (PL) spectroscopy is a standard technique used for studying the interfacial charge transfer properties of photovoltaic devices, including perovskites. By measuring the PL intensity of the photoactive layer with and without the charge transfer layers, one can in principle determine the fraction of charge carriers that are transferred across the interfaces and, if combined with time-resolved data, the rate constants for these charge transfers. The efficiency of these charge transfer processes is a key consideration for photocurrent generation in complete devices.

It is apparent from the data presented herein that measurement of the efficiency of electron transfer for $MAPI_3/PC_{61}BM$ bilayers and hole transfer for PEDOT:PSS/$MAPI_3$ bilayers is strongly dependent upon the excitation conditions employed. In particular, it is apparent that the PLQE measured in a standard photoluminescence spectrometer can yield significantly different transfer efficiencies to those measured under 1 Sun equivalent irradiation, due to the relatively low excitation conditions employed in standard spectrometers. Furthermore, transient spectroscopic measurements measured under pulsed laser excitation may also yield very different transfer efficiencies depending upon the excitation conditions employed. As we demonstrate, TCSPC measurements can yield relatively low transfer efficiencies due to the excitation densities being much lower than 1 Sun irradiation, and ultrafast transient absorption measurements can yield relatively low transfer efficiencies for the opposite reason of employing higher excitation density conditions than those relevant to 1 Sun irradiation.

The primary cause of this dependence of transfer efficiency upon excitation conditions is the dependence of charge trapping and recombination in $MAPI_3$ upon charge carrier density. It is already well established that the recombination dynamics

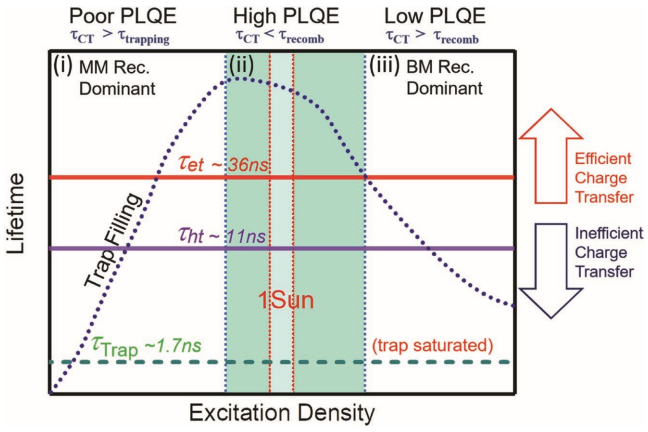

Figure 5. Illustration of the excitation density dependence of the competing interfacial charge transfer kinetics and yields versus charge trapping and recombination. *Y*-axis corresponds to measured charge lifetimes.

in $MAPI_3$ films is charge density dependent and can be dominated by Shockley–Read–Hall recombination to sub-bandgap trap states (1st order with respect to charge density) at low charge densities, by free electron–hole bimolecular recombination (2nd order with respect to charge density) at intermediate charge densities, and by Auger recombination (3rd order process) at very high charge densities.[3e,f,18b] We note that Auger recombination only becomes dominant at very high charge densities ($\geq 2 \times 10^{18}$–5×10^{18} cm^{-3}),[2e,21,25] outside the scope of this study. The transition from 1st to 2nd order recombination has been suggested to occur when the density of photogenerated charge carriers exceeds the trap density, resulting in a saturation of charge trapping.[3a–c]

The excitation density dependence of PLQE, and therefore charge transfer efficiencies, can be understood in terms of the charge carrier density dependence of charge trapping and recombination, as illustrated in **Figure 5**. At low excitation densities, nanosecond charge trapping processes compete effectively with charge transfer to the $PC_{61}BM$ and PEDOT:PSS layers, resulting in low PLQE's. At intermediate excitation densities, this charge trapping saturates due to trap filling, enabling efficient electron/hole transfer. This transition to efficient charge transfer occurs for the bilayers studied at steady-state light fluxes of ≈0.01 Sun or a charge density of $\approx 5 \times 10^{15}$ cm^{-3} from our pulsed laser measurements. As the excitation intensity, and resulting charge density, is increased further, bimolecular recombination accelerates and begins to compete with charge transfer for densities greater than $\approx 3 \times 10^{17}$ cm^{-3}. Under 1 Sun irradiation, hole transfer in PEDOT:PSS/$MAPI_3$ bilayer remains efficient, but the electron transfer efficiency in $MAPI_3$/$PC_{61}BM$ bilayers drops to ≈50%. At higher excitation conditions, both hole and, particularly, electron transfer efficiency drops further as bimolecular recombination accelerates.

From our TCSPC data, we estimate excitation density independent electron/hole transfer lifetimes of ≈36 and 11 ns, respectively. We note these measured time constants for electron and hole transfer may be limited by either charge transport to the bilayer interfaces or by electron/hole transfer at these interfaces. In this regard, the faster time constant for the PEDOT:PSS/$MAPI_3$ bilayer is consistent with the higher hole mobility reported for $MAPI_3$ relative to its electron mobility, and with the higher PLQE we observe for this bilayer.[26] Literature data for these charge transfer times to $PC_{61}BM$ and PEDOT:PSS are in the range of 0.4–15 and of 6–90 ns for electron and hole transfer, respectively.[4d,27] It is not clear if these variations reflects variations in sample preparation, measurement technique or excitation density. We note that some of these measurements employed very low excitation conditions where competition with charge trapping is likely to be critical. We also note that most studies measured kinetics on films shortly after fabrication, where the subsequent evolution of film photoluminescence, and therefore $MAPI_3$ photophysics, with storage and/or light exposure time may have significant impact. We further note that our TCSPC measurements at low excitation densities indicate that charge trapping kinetics are not changed by the presence of $PC_{61}BM$ and PEDOT:PSS contact layers, indicating that neither contact layer generates a significant number of surface defects/recombination centers.

As discussed above, our PLQE data as a function of pulse energy indicate that charge trapping no longer competes effectively with charge transfer for excitation densities of $\approx 10^{16}$ cm^{-3}. Indeed, increasing the excitation density to only 3×10^{15} cm^{-3} already results in an increase in PLQE, and therefore charge transfer efficiency, to 40% (Figure 3b). These data suggest that these relatively low excitation densities are sufficient to result in enough trap filling to enable efficient charge transfer.[28] These data, however, contrast with other assays of trap density in $MAPI_3$ films, based on for example analysis of steady-state photoluminescence versus light flux, which more typically yield trap densities of $\approx 10^{17}$ cm^{-3}.[2d,19a] The origin of this apparent discrepancy is not fully determined. However there is likely to be a distribution of trap depths in $MAPI_3$ films, as we and others have discussed in refs. [5h], [20], and [29], with charge trapping being relatively irreversible for deeper traps, but more reversible (on the nanosecond timescale relevant to charge transfer) for shallower trap states (sometimes referred to as "tail states"). It appears reasonable that trapping into a relatively low density of deeper traps competes effectively with charge transfer, whilst the presence of a higher density of shallow tail states, whilst impacting upon PL density, has relatively little impact upon the efficiency of charge transfer.

The steady-state PLQE versus light flux plot in Figure 2b shows a drop in PLQE from ≈84% to 55% between 0.1% and 1% of 1 Sun for in $MAPI_3$/$PC_{61}BM$ bilayers. An equivalent drop in PLQE is not observed in the low repetition rate pulsed PLQE measurements (Figure 3b). Whilst a quantitative comparison between steady-state and pulsed measurements is challenging, it appears most likely that this drop in PLQE at modest steady-state light fluxes is associated with charge accumulation in the $PC_{61}BM$ layer impeding electron transfer in the steady-state measurements. In the pulsed measurements, where the bilayers recover to their dark charge densities between light pulses, such charge accumulation will have less impact. We note that such charge accumulation is likely to be particularly important in complete devices under open circuit conditions, and less critical at short circuit where charges are extracted to the external circuit. However, study of such issues requires data on complete devices, beyond the scope of this study.

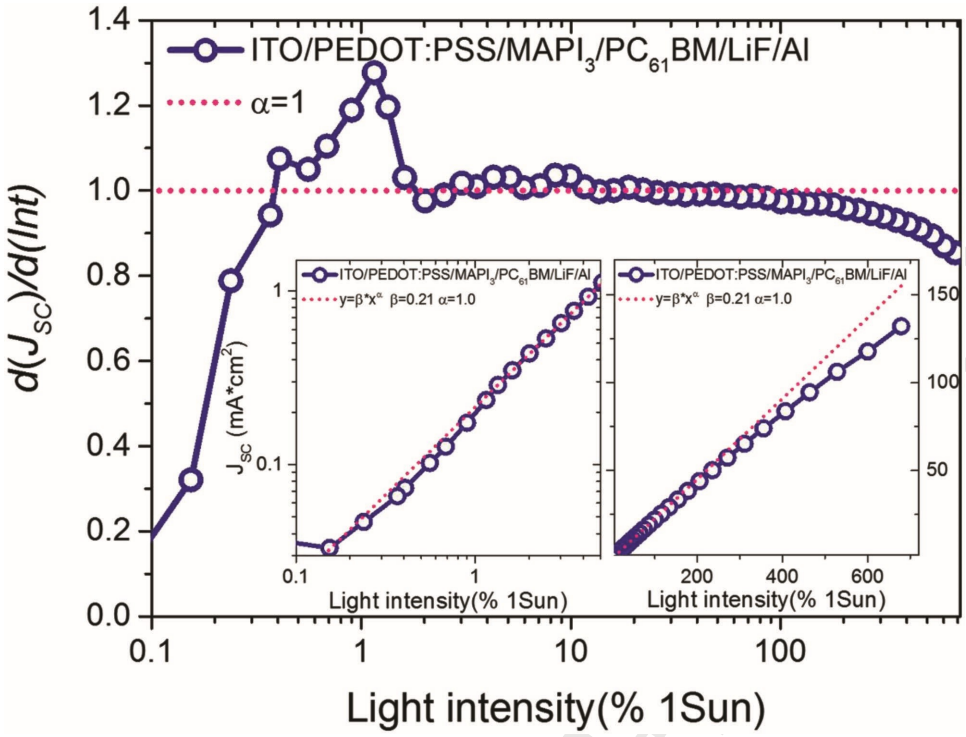

Figure 6. Linearity of J_{SC} versus excitation light intensity (Int) for an ITO/PEDOT:PSS/$MAPI_3$/PC_{61}BM/LiF/Al device, shown in the insets as direct dependencies for low and high excitation densities as a function of light intensity and as $d(J_{SC})/d(Int)$ versus Int in the main figure.

We conclude with a brief discussion of the relevance of the data reported herein to the operation of complete devices under steady-state irradiation. The current study is limited to bilayers, and therefore cannot be directly compared to complete devices. However, at least qualitatively, photocurrent generation in analogous complete devices can be expected to show similar trends to those reported herein, with irreversible charge trapping limiting photocurrent generation at very low light fluxes, and bimolecular recombination limiting photocurrent generation at high light fluxes. Details of this behavior will depend upon contact layer, $MAPI_3$ layer thickness and processing, device operating condition and field distribution, amongst other parameters. As an initial evaluation of this issue, **Figure 6** presents a plot of $d(J_{SC})/d(Int)$ as a function of l light intensity (Int), where the J_{SC} is measured of a complete Glass/ITO/PEDOT:PSS/$MAPI_3$/PC_{61}BM/LiF/Al device. $d(J_{SC})/d(Int)$ values <1 are a measure of the presence of nonlinear losses limiting photocurrent generation.[30] It is striking that PLQE and $d(J_{SC})/d(Int)$ show rather analogous dependencies on light intensity (compare Figures 2b and 3a to Figure 6), indicating that the effects discussed on bilayers are directly relevant to complete device performance, with the intensity dependence of interfacial charge transfer impacting directly upon the intensity dependence of photocurrent generation. We are currently undertaking more quantitative analysis of this issue, including direct measurements of transfer efficiencies in complete devices, to determine the detailed impact of these dependencies upon device performance. In particular, we note that the study herein does not address the issue of whether charges transferred to the contact layers are efficiently extracted to the external circuit (not present in the bilayer samples studied herein) or undergo surface recombination losses, a key consideration for many MAPI solar cells.

4. Conclusion

We find that different experimental assays of charge transfer efficiency in $MAPI_3$/PC_{61}BM and PEDOT:PSS/$MAPI_3$ films can yield very different results. We link these differences to the excitation conditions employed in terms of excitation density and pulsed versus steady-state measurements. We find that PLQE measurements in a typical PL spectrometer can yield significantly higher transfer efficiencies to those measured under 1 Sun irradiation. To ensure most relevance to device operation, we conclude that such steady-state PLQE measurements should be done using irradiation conditions similar to solar irradiation. We further find that typical TCSPC transient emission studies and ultrafast transient absorption studies yield transfer efficiencies very different from those observed under 1 Sun conditions due to the different excitation conditions typically employed in such studies. Electron and hole transfer times to PC_{61}BM and PEDOT:PSS are determined to be 36 and 11 ns, respectively, for the films studied. The slower transfer time for electrons results in a stronger dependence of transfer efficiency upon excitation conditions. From pulsed excitation measurements, we find that excitation densities of $\approx 5 \times 10^{15}$ cm^{-3} are sufficient to reach the highest charge transfer efficiencies, indicating that the density of traps in $MAPI_3$ which compete directly with charge transfer is of this order of magnitude. At higher excitation conditions, accelerating

bimolecular recombination is observed to reduce charge transfer efficiencies. The measured excitation density dependencies of charge transfer efficiency in these bilayers are shown to correlate, at least qualitatively, with the linearity of device photocurrent with light intensity, indicating the relevance of the charge carrier dependent transfer process in operational devices.

5. Experimental Section

Sample Preparation—Perovskite Layer: $MAPI_3$ ($CH_3NH_3PbI_3$) from Toluene Dripping Method: All chemicals were purchased from commercial suppliers. The $CH_3NH_3PbI_3$ perovskite precursor solutions were prepared in ambient conditions but the films were deposited in a N_2 filled glove box (O_2 and H_2O level below 0.5 ppm). For the precursor solution, 199 mg mL^{-1} of methylammonium iodide (Dyesol, PN101000) and 576 mg mL^{-1} of PbI_2 (Sigma-Aldrich, 99%) were dissolved in 7:3 volume ratio in GBL (Aldrich, 99%) and DMSO (Fluka, 99%) mixed solution, and then stirred for 3 h at 65 °C. The γ-butyrolactone and dimethyl sulfoxide solvents were dehydrated using magnesium sulfate (VWR chemicals) prior to their use. The precursor solution was filtered through a 0.2 µm PTFE filter and then pipetted onto a cleaned and oxygen plasma pretreated soda-lime glass substrate (substrate area ≈ 2.5 cm × 2.5 cm) (VWR chemicals). The film was sequentially spun for 5 s at 1000 rpm, for 10 s at 1000 rpm, for 19 s at 4000 rpm, and for 5 s at 500 rpm, during which toluene (700 µL) was quickly dropped in the center of the substrate, and finally spun for 50 s at 4000 rpm. The samples were then annealed at 100 °C for 10 min.

Sample Preparation—Hole Transport Layer: PEDOT:PSS: PEDOT:PSS (Clevios P VP AI4083) was filtered through a 0.45 µm filter and spin cast on oxygen plasma pretreated substrate at 3500 rpm for 45 s. The sample was dried on a hotplate at 150 °C for 15 min in air. Before deposition of the perovskite layer, the PEDOT:PSS substrate was annealed for 5 min at 150 °C in a glove box.

Sample Preparation—Electron Transport Layer: PC61BM: [6,6]-Phenyl-C_{61}-butyricacidmethyleater ($PC_{61}BM$) (Nano C) (20 mg mL^{-1}) dissolved in anhydrous chlorobenzene (Sigma-Aldrich, 99.8%) was deposited onto a predeposited perovskite film at 2000 rpm for 60 s and then 4000 rpm for 10 s. The film was then left to dry for an hour in the glove box.

Sample Preparation—Device Fabrication: For complete devices structure Glass/ITO/PEDOT:PSS/$MAPI_3$/$PC_{61}BM$/LiF/Al an "inverted planar" device was employed. Well cleaned patterned ITO coated glass slides (Psiotec) were employed as substrates and then treated with oxygen plasma for 7 min. PEDOT:PSS, $MAPI_3$, and $PC_{61}BM$ layers were spin coated on the substrate in the order following the above conditions. Finally, a 10 nm LiF and 100 nm Al top cathode layer was deposited through a patterned shadow mask by thermal evaporation at ≈10^{-7} mbar high vacuum with a deposition rate of 0.2 nm s^{-1}. The device active area size is 0.045 cm^{-2} (0.3 × 0.15 cm^{-2}). *J*/*V* curve was measured using a Xenon lamp at 1 Sun AM1.5 solar illumination (Oriel Instruments) calibrated to a silicon reference cell prior to perform with a source meter (Keithley 2400). Scan rates were 0.125 V s^{-1}. Light intensity dependent short-circuit current density (J_{sc}) was measured with a white light emitting diode with tunable power supply.

Sample Preparation—Sample Encapsulation: All the samples were encapsulated in a nitrogen-filled glove box to prevent degradation by air during spectroscopic experiments using a glass coverslip and Surlyn (Solaronix, Switzerland). The seal was cured by heating to ≈100 °C the gasket around the cell with the tip of a soldering iron. After this epoxy glue was applied to seal more completely the edge of the glass and coverslip.

Film Characterization—Spectroscopy: All samples were kept for 12 d in a nitrogen-filled glove box at room temperature and in the dark before spectroscopy measurements to avoid the occurrence of surface reconstruction and ripening effects during experiments.[31] The photoluminescence spectra were recorded using Fluoromax 3 (Horiba Jobin Yvon) and the absorption spectra using Shimadazu UV-2600. The optical stability of the samples was checked before and after TAS and TCSPC experiments by recording their photoluminescence and absorption spectra.

Film Characterization—Ultrafast fs-TAS: Ultrafast transient absorption spectra were recorded using an HELIOS transient absorption spectrometer (Ultrafast systems) with a 715 nm excitation source generated by an optical parametric amplifier (TOPAS Prime, Spectra-Physics) and a frequency mixer (NirUVis, Light Conversion) and a probe pulse generated in a sapphire crystal. These were seeded by a Solstice Ti:Sapphire regenerative amplifier (Newport, Spectra-Physics), with a resulting system instrument response time of 200 fs. The excitation density of the pump beam was modulated using a graded neutral density filter from 0.25 to 50 µJ cm^{-2} pulse energies at a repetition rate of 500 Hz, monitored with a VEGA energy meter (OPHIR Photonics). Data analysis was conducted using Origin software.

Film Characterization—TCSPC: For TCSPC measurements of transient photoluminescence, a Delta Flex system (Horiba Scientific) was used. The excitation was a 635 nm diode laser of <200 ps pulse duration (NanoLED N-02B, Horiba scientific) with a 1 MHz repetition rate. Neutral density filters were used to modulate the excitation pulse energies from 5.7 to 178 pJ cm^{-2}, corresponding to 0.004 to 0.13 mW cm^{-2} average power densities. PL transient signal was collected using a single-photon counting detectors (PPD-900, Horiba scientific) with 100 ns time window.

Film Characterization—Steady-State Photoluminescence Spectroscopy: Steady-state PL measurements were conducted using a range of light sources in an FL 1039 spectrometer (Horiba Scientific). Fixed intensity measurements were undertaken using 635 nm excitation generated from the spectrometer's internal xenon light source with intensity ≈1.5 mW cm^{-2}. For variable excitation density white light irradiation, an external white LED light source (Bridgelux RS Array BXRA-40E7500-j-03) was employed with 650 and 700 nm short wavelength pass filters (see Figure S13, Supporting Information, for irradiation spectrum). The excitation fluence was manipulated using the DC power supply for the LED from 0.08 to 370% of 1 Sun, and PL from the sample was collected by passing through a 650 nm long pass filter in order to cut off the excitation light source.

Film Characterization—Nanosecond Pulsed Photoluminescence Measurements: Photoluminescence quantum yields using higher intensity excitation pulses compared to the TCSPC measurements were recorded using a Nd:YAG pumped Opolette (OPOTEK) laser source for excitation at 635 nm and a 1 mm diameter Si-photodiode detector housed in a Constronics preamplifier for detection, corresponding to 380 to 0.1 µJ cm^{-2} pulse energies at a repetition rate of 20 Hz. The resulting PL transients were measured with 100 ns instrument response time, recording only the peak PL intensity.

Supporting Information

Supporting Information is available from the Wiley Online Library or from the author.

Acknowledgements

The authors gratefully acknowledge funding from the GCRF EPSRC project SUNRISE (EP/P032591/1) and Welsh Government Sêr Cymru Solar projects. This work was part-funded by the European regional Development Fund through the Welsh Government. T.D. acknowledges receipt of CSC funding and the authors thank Dr. Xiaoe Li for technical support.

Conflict of Interest

The authors declare no conflict of interest.

Keywords

charge carrier dynamics, interfacial charge transfer, perovskite solar cells, photoluminescence spectroscopy, transient optical spectroscopies

Received: August 9, 2018
Revised: October 1, 2018
Published online:

[1] a) NREL, Best Research-Cell Efficiencies, https://www.nrel.gov/pv/assets/images/efficiency-chart.png (accessed: July 2018); b) A. Kojima, K. Teshima, Y. Shirai, T. Miyasaka, *J. Am. Chem. Soc.* **2009**, *131*, 6050; c) X. Li, D. Bi, C. Yi, J. D. Decoppet, J. Luo, S. M. Zakeeruddin, A. Hagfeldt, M. Gratzel, *Science* **2016**, *353*, 58; d) Y. Rong, Z. Tang, Y. Zhao, X. Zhong, S. Venkatesan, H. Graham, M. Patton, Y. Jing, A. M. Guloy, Y. Yao, *Nanoscale* **2015**, *7*, 10595; e) S. S. Shin, E. J. Yeom, W. S. Yang, S. Hur, M. G. Kim, J. Im, J. Seo, J. H. Noh, S. I. Seok, *Science* **2017**, *356*, 167; f) M. Saliba, T. Matsui, J. Y. Seo, K. Domanski, J. P. Correa-Baena, M. K. Nazeeruddin, S. M. Zakeeruddin, W. Tress, A. Abate, A. Hagfeldt, M. Gratzel, *Energy Environ. Sci.* **2016**, *9*, 1989; g) Q. Chen, H. Zhou, Z. Hong, S. Luo, H. S. Duan, H. H. Wang, Y. Liu, G. Li, Y. Yang, *J. Am. Chem. Soc.* **2014**, *136*, 622; h) H. Sun, K. Deng, Y. Zhu, M. Liao, J. Xiong, Y. Li, L. Li, *Adv. Mater.* **2018**, https://doi.org/10.1002/adma.201801935e1801935; i) M. M. Tavakoli, P. Yadav, R. Tavakoli, J. Kong, *Adv. Energy Mater.* **2018**, https://doi.org/10.1002/aenm.2018007941800794.

[2] a) J. H. Im, C. R. Lee, J. W. Lee, S. W. Park, N. G. Park, *Nanoscale* **2011**, *3*, 4088; b) S. D. Stranks, G. E. Eperon, G. Grancini, C. Menelaou, M. J. Alcocer, T. Leijtens, L. M. Herz, A. Petrozza, H. J. Snaith, *Science* **2013**, *342*, 341; c) G. Xing, N. Mathews, S. Sun, S. S. Lim, Y. M. Lam, M. Gratzel, S. Mhaisalkar, T. C. Sum, *Science* **2013**, *342*, 344; d) G. Xing, N. Mathews, S. S. Lim, N. Yantara, X. Liu, D. Sabba, M. Gratzel, S. Mhaisalkar, T. C. Sum, *Nat. Mater.* **2014**, *13*, 476; e) M. Cadelano, V. Sarritzu, N. Sestu, D. Marongiu, F. Chen, R. Piras, R. Corpino, C. M. Carbonaro, F. Quochi, M. Saba, A. Mura, G. Bongiovanni, *Adv. Opt. Mater.* **2015**, *3*, 1557.

[3] a) S. Draguta, S. Thakur, Y. V. Morozov, Y. Wang, J. S. Manser, P. V. Kamat, M. Kuno, *J. Phys. Chem. Lett.* **2016**, *7*, 715; b) S. D. Stranks, V. M. Burlakov, T. Leijtens, J. M. Ball, A. Goriely, H. J. Snaith, *Phys. Rev. Appl.* **2014**, 2; c) Z. Y. Zhang, H. Y. Wang, Y. X. Zhang, Y. W. Hao, C. Sun, Y. Zhang, B. R. Gao, Q. D. Chen, H. B. Sun, *Sci. Rep.* **2016**, *6*, 27286; d) J. Q. Grim, S. Christodoulou, F. Di Stasio, R. Krahne, R. Cingolani, L. Manna, I. Moreels, *Nat. Nanotechnol.* **2014**, *9*, 891; e) C. Wehrenfennig, G. E. Eperon, M. B. Johnston, H. J. Snaith, L. M. Herz, *Adv. Mater.* **2014**, *26*, 1584; f) M. B. Johnston, L. M. Herz, *Acc. Chem. Res.* **2016**, *49*, 146; g) R. L. Milot, G. E. Eperon, H. J. Snaith, M. B. Johnston, L. M. Herz, *Adv. Funct. Mater.* **2015**, *25*, 6218.

[4] a) Q. Shen, Y. Ogomi, J. Chang, S. Tsukamoto, K. Kukihara, T. Oshima, N. Osada, K. Yoshino, K. Katayama, T. Toyoda, S. Hayase, *Phys. Chem. Chem. Phys.* **2014**, *16*, 19984; b) S. Makuta, M. Liu, M. Endo, H. Nishimura, A. Wakamiya, Y. Tachibana, *Chem. Commun.* **2016**, *52*, 673; c) P. Piatkowski, B. Cohen, F. Javier Ramos, M. Di Nunzio, M. K. Nazeeruddin, M. Gratzel, S. Ahmad, A. Douhal, *Phys. Chem. Chem. Phys.* **2015**, *17*, 14674; d) E. M. Hutter, J. J. Hofman, M. L. Petrus, M. Moes, R. D. Abellon, P. Docampo, T. J. Savenije, *Adv. Energy Mater.* **2017**, *7*, 1602349.

[5] a) G. J. Hedley, A. J. Ward, A. Alekseev, C. T. Howells, E. R. Martins, L. A. Serrano, G. Cooke, A. Ruseckas, I. D. Samuel, *Nat. Commun.* **2013**, *4*, 2867; b) A. J. Ward, A. Ruseckas, M. M. Kareem, B. Ebenhoch, L. A. Serrano, M. Al-Eid, B. Fitzpatrick, V. M. Rotello, G. Cooke, I. D. Samuel, *Adv. Mater.* **2015**, *27*, 2496; c) K. H. Lee, P. E. Schwenn, A. R. Smith, H. Cavaye, P. E. Shaw, M. James, K. B. Krueger, I. R. Gentle, P. Meredith, P. L. Burn, *Adv. Mater.* **2011**, *23*, 766; d) J. Kim, I. Heo, D. Park, S. J. Ahn, S. Y. Jang, S. Yim, *J. Mater. Chem. A* **2014**, *2*, 10250; e) Z. Tan, J. Li, C. Zhang, Z. Li, Q. Hu, Z. Xiao, T. Kamiya, H. Hosono, G. Niu, E. Lifshitz, Y. Cheng, J. Tang, *Adv. Funct. Mater.* **2018**, https://doi.org/10.1002/adfm.2018011311801131; f) Y. Q. Luo, S. Aharon, M. Stuckelberger, E. Magana, B. Lai, M. I. Bertoni, L. Etgar, D. P. Fenning, *Adv. Funct. Mater.* **2018**, *28*, 1706995; g) F. Zhang, W. Shi, J. Luo, N. Pellet, C. Yi, X. Li, X. Zhao, T. J. S. Dennis, X. Li, S. Wang, Y. Xiao, S. M. Zakeeruddin, D. Bi, M. Gratzel, *Adv. Mater.* **2017**, 29; h) Y. Lin, L. Shen, J. Dai, Y. Deng, Y. Wu, Y. Bai, X. Zheng, J. Wang, Y. Fang, H. Wei, W. Ma, X. C. Zeng, X. Zhan, J. Huang, *Adv. Mater.* **2017**, 29; i) C. M. Wolff, F. Zu, A. Paulke, L. P. Toro, N. Koch, D. Neher, *Adv. Mater.* **2017**, 29; j) J. R. Zhang, D. L. Bai, Z. W. Jin, H. Bian, K. Wang, J. Sun, Q. Wang, S. Z. Liu, *Adv. Energy Mater.* **2018**, *8*, 1703246; k) B. Krogmeier, F. Staub, D. Grabowski, U. Rau, T. Kirchartz, *Sustainable Energy Fuels* **2018**, *2*, 1027; l) F. Staub, T. Kirchartz, K. Bittkau, U. Rau, *J. Phys. Chem. Lett.* **2017**, *8*, 5084.

[6] a) D. S. Ginger, N. C. Greenham, *Phys. Rev. B* **1999**, *59*, 10622; b) K. Cnops, B. P. Rand, D. Cheyns, B. Verreet, M. A. Empl, P. Heremans, *Nat. Commun.* **2014**, *5*, 3406; c) D. M. Stoltzfus, J. E. Donaghey, A. Armin, P. E. Shaw, P. L. Burn, P. Meredith, *Chem. Rev.* **2016**, *116*, 12920.

[7] P. Docampo, J. M. Ball, M. Darwich, G. E. Eperon, H. J. Snaith, *Nat. Commun.* **2013**, *4*, 2761.

[8] K. Tvingstedt, L. Gil-Escrig, C. Momblona, P. Rieder, D. Kiermasch, M. Sessolo, A. Baumann, H. J. Bolink, V. Dyakonov, *ACS Energy Lett.* **2017**, *2*, 424.

[9] a) J. You, L. Meng, T. B. Song, T. F. Guo, Y. M. Yang, W. H. Chang, Z. Hong, H. Chen, H. Zhou, Q. Chen, Y. Liu, N. De Marco, Y. Yang, *Nat. Nanotechnol.* **2016**, *11*, 75; b) H. T. Peng, W. H. Sun, Y. L. Li, W. B. Yan, P. R. Yu, H. P. Zhou, Z. Q. Bian, C. H. Huang, *J. Photonics Energy* **2016**, *6*, 022002.

[10] a) X. F. Deng, X. M. Wen, J. H. Zheng, T. Young, C. F. J. Lau, J. Kim, M. Green, S. J. Huang, A. Ho-Baillie, *Nano Energy* **2018**, *46*, 356; b) D. W. deQuilettes, W. Zhang, V. M. Burlakov, D. J. Graham, T. Leijtens, A. Osherov, V. Bulovic, H. J. Snaith, D. S. Ginger, S. D. Stranks, *Nat. Commun.* **2016**, *7*, 11683; c) X. Feng, H. Su, Y. Wu, H. Wu, J. Xie, X. Liu, J. Fan, J. Dai, Z. He, *J. Mater. Chem. A* **2017**, *5*, 12048; d) D. W. deQuilettes, S. M. Vorpahl, S. D. Stranks, H. Nagaoka, G. E. Eperon, M. E. Ziffer, H. J. Snaith, D. S. Ginger, *Science* **2015**, *348*, 683; e) L. Zuo, H. Guo, D. W. deQuilettes, S. Jariwala, N. De Marco, S. Dong, R. DeBlock, D. S. Ginger, B. Dunn, M. Wang, Y. Yang, *Sci. Adv.* **2017**, *3*, e1700106; f) T. Li, Y. Pan, Z. Wang, Y. Xia, Y. Chen, W. Huang, *J. Mater. Chem. A* **2017**, *5*, 12602; g) A. R. Pascoe, S. Meyer, W. Huang, W. Li, I. Benesperi, N. W. Duffy, L. Spiccia, U. Bach, Y.-B. Cheng, *Adv. Funct. Mater.* **2016**, *26*, 1278.

[11] a) H. Choi, C. K. Mai, H. B. Kim, J. Jeong, S. Song, G. C. Bazan, J. Y. Kim, A. J. Heeger, *Nat. Commun.* **2015**, *6*, 7348; b) K. C. Wang, J. Y. Jeng, P. S. Shen, Y. C. Chang, E. W. Diau, C. H. Tsai, T. Y. Chao, H. C. Hsu, P. Y. Lin, P. Chen, T. F. Guo, T. C. Wen, *Sci. Rep.* **2014**, *4*, 4756; c) Y. Wu, X. Yang, W. Chen, Y. Yue, M. Cai, F. Xie, E. Bi, A. Islam, L. Han, *Nat. Energy* **2016**, *1*, 16148; d) K. Gao, B. Xu, C. Hong, X. Shi, H. Liu, X. Li, L. Xie, A. K. Y. Jen, *Adv. Energy Mater.* **2018**, https://doi.org/10.1002/aenm.2018008091800809; e) Y.-Q. Zhou, B.-S. Wu, G.-H. Lin, Z. Xing, S.-H. Li, L.-L. Deng, D.-C. Chen, D.-Q. Yun, S.-Y. Xie, *Adv. Energy Mater.* **2018**, https://doi.org/10.1002/aenm.2018003991800399; f) W. Chen, Y. Wu, J. Fan, A. B. Djurišić, F. Liu, H. W. Tam, A. Ng, C. Surya, W. K. Chan, D. Wang, Z.-B. He, *Adv. Energy Mater.* **2018**, *8*, 1703519.

[12] a) J. J. Chang, H. Zhu, B. C. Li, F. H. Isikgor, Y. Hao, Q. H. Xu, J. Y. Ouyang, *J. Mater. Chem. A* **2016**, *4*, 887; b) C. L. Chuang, C.-Y. Chen, C.-H. Chiang, C.-G. Wu, *Inorg. Chem. Front.* **2017**, *4*, 850;

c) A. Matas Adams, J. M. Marin-Beloqui, G. Stoica, E. Palomares, *J. Mater. Chem. A* **2015**, *3*, 22154.

[13] a) Q. F. Xue, M. Y. Liu, Z. C. Li, L. Yan, Z. C. Hu, J. W. Zhou, W. Q. Li, X. F. Jiang, B. M. Xu, F. Huang, Y. Li, H. L. Yip, Y. Cao, *Adv. Funct. Mater.* **2018**, *28*, 1707444; b) H. Dong, Z. X. Wu, J. Xi, X. B. Xu, L. J. Zuo, T. Lei, X. G. Zhao, L. J. Zhang, X. Hou, A. K. Y. Jen, *Adv. Funct. Mater.* **2018**, *28*, 1704836; c) A. N. Cho, N. G. Park, *ChemSusChem* **2017**, *10*, 3687; d) G. Y. Xu, R. M. Xue, W. J. Chen, J. W. Zhang, M. Y. Zhang, H. Y. Chen, C. H. Cui, H. K. Li, Y. W. Li, Y. F. Li, *Adv. Energy Mater.* **2018**, *8*, 1703054; e) H. Hao, L. Wang, X. Ma, K. Cao, H. Yu, M. Wang, W. Gu, R. Zhu, M. S. Anwar, S. Chen, W. Huang, *Sol. RRL* **2018**, https://doi.org/10.1002/solr.2018000611800061.

[14] a) T. Du, C. H. Burgess, J. Kim, J. Q. Zhang, J. R. Durrant, M. A. McLachlan, *Sustainable Energy Fuels* **2017**, *1*, 119; b) D. Bryant, N. Aristidou, S. Pont, I. Sanchez-Molina, T. Chotchunang atchaval, S. Wheeler, J. R. Durrant, S. A. Haque, *Energy Environ. Sci.* **2016**, *9*, 1655.

[15] a) N. J. Jeon, J. H. Noh, Y. C. Kim, W. S. Yang, S. Ryu, S. I. Seok, *Nat. Mater.* **2014**, *13*, 897; b) N. G. Park, M. Gratzel, T. Miyasaka, K. Zhu, K. Emery, *Nat. Energy* **2016**, *1*, 16152; c) Y. Z. Wu, A. Islam, X. D. Yang, C. J. Qin, J. Liu, K. Zhang, W. Q. Peng, L. Y. Han, *Energy Environ. Sci.* **2014**, *7*, 2934.

[16] a) O. Malinkiewicz, A. Yella, Y. H. Lee, G. M. Espallargas, M. Graetzel, M. K. Nazeeruddin, H. J. Bolink, *Nat. Photonics* **2013**, *8*, 128; b) B. Xia, Z. X. Wu, H. Dong, J. Xi, W. Wu, T. Lei, K. Xi, F. Yuan, B. Jiao, L. X. Xiao, Q. H. Gong, X. Hou, *J. Mater. Chem. A* **2016**, *4*, 6295.

[17] E. M. Talbert, H. F. Zarick, N. J. Orfield, W. Li, W. R. Erwin, Z. R. DeBra, K. R. Reid, C. P. McDonald, J. R. McBride, J. Valentine, S. J. Rosenthal, R. Bardhan, *RSC Adv.* **2016**, *6*, 86947.

[18] a) F. Vietmeyer, P. A. Frantsuzov, B. Janko, M. Kuno, *Phys. Rev. B* **2011**, 83; b) M. Saba, M. Cadelano, D. Marongiu, F. Chen, V. Sarritzu, N. Sestu, C. Figus, M. Aresti, R. Piras, A. G. Lehmann, C. Cannas, A. Musinu, F. Quochi, A. Mura, G. Bongiovanni, *Nat. Commun.* **2014**, *5*, 5049.

[19] a) X. Wen, Y. Feng, S. Huang, F. Huang, Y.-B. Cheng, M. Green, A. Ho-Baillie, *J. Mater. Chem. C* **2016**, *4*, 793; b) Y. Yamada, T. Yamada, A. Shimazaki, A. Wakamiya, Y. Kanemitsu, *J. Phys. Chem. Lett.* **2016**, *7*, 1972.

[20] S. Wheeler, D. Bryant, J. Troughton, T. Kirchartz, T. Watson, J. Nelson, J. R. Durrant, *J. Phys. Chem. C* **2017**, *121*, 13496.

[21] M. Cadelano, M. Saba, N. Sestu, V. Sarritzu, D. Marongiu, F. Chen, R. Piras, F. Quochi, A. Mura, G. Bongiovanni, **2016**, https://doi.org/10.5772/61282.

[22] a) V. sharma, S. Aharon, I. Gdor, C. Yang, L. Etgar, S. Ruhman, *J. Mater. Chem. A* **2016**, *4*, 3546; b) J. M. Marin-Beloqui, J. P. Hernandez, E. Palomares, *Chem. Commun.* **2014**, *50*, 14566; c) A. Marchioro, J. Teuscher, D. Friedrich, M. Kunst, R. van de Krol, T. Moehl, M. Gratzel, J. E. Moser, *Nat. Photonics* **2014**, *8*, 250; d) H. S. Kim, C. R. Lee, J. H. Im, K. B. Lee, T. Moehl, A. Marchioro, S. J. Moon, R. Humphry-Baker, J. H. Yum, J. E. Moser, M. Gratzel, N. G. Park, *Sci. Rep.* **2012**, *2*, 591.

[23] a) T. C. Sum, N. Mathews, G. Xing, S. S. Lim, W. K. Chong, D. Giovanni, H. A. Dewi, *Acc. Chem. Res.* **2016**, *49*, 294; b) J. S. Manser, P. V. Kamat, *Nat. Photonics* **2014**, *8*, 737.

[24] R. Godin, X. R. Ma, S. Gonzalez-Carrero, T. Du, X. E. Li, C. T. Lin, M. A. McLachlan, R. E. Galian, J. Perez-Prieto, J. R. Durrant, *Adv. Opt. Mater.* **2018**, *6*, 1701203.

[25] T. C. Sum, N. Mathews, *Energy Environ. Sci.* **2014**, *7*, 2518.

[26] a) T. Zhao, W. Shi, J. Xi, D. Wang, Z. Shuai, *Sci. Rep.* **2016**, *7*, 19968; b) Q. Dong, Y. Fang, Y. Shao, P. Mulligan, J. Qiu, L. Cao, J. Huang, *Science* **2015**, *347*, 967; c) Y. Chen, J. Peng, D. Su, X. Chen, Z. Liang, *ACS Appl. Mater. Interfaces* **2015**, *7*, 4471; d) J. Peng, Y. Chen, K. Zheng, T. Pullerits, Z. Liang, *Chem. Soc. Rev.* **2017**, *46*, 5714.

[27] a) T. Jiang, W. Fu, *RSC Adv.* **2018**, *8*, 5897; b) E. Bi, H. Chen, F. Xie, Y. Wu, W. Chen, Y. Su, A. Islam, M. Gratzel, X. Yang, L. Han, *Nat. Commun.* **2017**, *8*, 15330; c) J. C. Yu, J. A. Hong, E. D. Jung, D. B. Kim, S. M. Baek, S. Lee, S. Cho, S. S. Park, K. J. Choi, M. H. Song, *Sci. Rep.* **2018**, *8*, 1070; d) C. Li, F. Wang, J. Xu, J. Yao, B. Zhang, C. Zhang, M. Xiao, S. Dai, Y. Li, Z. Tan, *Nanoscale* **2015**, *7*, 9771; e) W. Zhang, Y. Ding, Y. Jiang, M. Zheng, S. Wu, X. Lu, M. Zeng, X. Gao, Q. Wang, G. Zhou, J.-m. Liu, K. Kempa, J. Gao, *RSC Adv.* **2017**, *7*, 39523; f) F. H. Isikgor, B. Li, H. Zhu, Q. Xu, J. Ouyang, *J. Mater. Chem. A* **2016**, *4*, 12543; g) C. Li, Y. Zhong, C. A. Luna, T. Unger, K. Deichsel, A. Graser, J. Kohler, A. Kohler, R. Hildner, S. Huettner, *Molecules* **2016**, 21; h) Y. Li, L. Meng, Y. M. Yang, G. Xu, Z. Hong, Q. Chen, J. You, G. Li, Y. Yang, Y. Li, *Nat. Commun.* **2016**, *7*, 10214.

[28] a) G. J. Nan, X. Zhang, M. Abdi-Jalebi, Z. Andaji-Garmaroudi, S. D. Stranks, G. Lu, D. Beljonne, *Adv. Energy Mater.* **2018**, *8*, 1702754; b) F. Staub, H. Hempel, J. C. Hebig, J. Mock, U. W. Paetzold, U. Rau, T. Unold, T. Kirchartz, *Phys. Rev. Appl.* **2016**, 6.

[29] a) Y. Wang, X. Sun, Z. Chen, Y. Y. Sun, S. Zhang, T. M. Lu, E. Wertz, J. Shi, *Adv. Mater.* **2017**, 29; b) T. Du, J. Kim, J. Ngiam, S. Xu, P. R. Barnes, J. R. Durrant, M. McLachlan, *Adv. Funct. Mater.* **2018**, https://doi.org/10.1002/201801808.

[30] a) L. J. A. Koster, V. D. Mihailetchi, H. Xie, P. W. M. Blom, *Appl. Phys. Lett.* **2005**, *87*, 203502; b) D. Fernandez, A. Viterisi, J. W. Ryan, F. Gispert-Guirado, S. Vidal, S. Filippone, N. Martin, E. Palomares, *Nanoscale* **2014**, *6*, 5871; c) J. Jimenez-Lopez, W. Cambarau, L. Cabau, E. Palomares, *Sci. Rep.* **2017**, *7*, 6101; d) K. Wang, C. Yi, C. Liu, X. Hu, S. Chuang, X. Gong, *Sci. Rep.* **2015**, *5*, 9265.

[31] a) Y. Yamada, M. Endo, A. Wakamiya, Y. Kanemitsu, *J. Phys. Chem. Lett.* **2015**, *6*, 482; b) Y. Tian, M. Peter, E. Unger, M. Abdellah, K. Zheng, T. Pullerits, A. Yartsev, V. Sundstrom, I. G. Scheblykin, *Phys. Chem. Chem. Phys.* **2015**, *17*, 24978.

ADVANCED ENERGY MATERIALS

Reprint Order Form 2018
- please return with your proofs -

Editorial Office:

Wiley-VCH Verlag, Boschstrasse 12
69469 Weinheim, Germany

Tel.: (+49) 6201 606 531
Fax: (+49) 6201 606 500

E-mail: advenergymat@wiley-vch.de
http://www.advenergymat.de

Manuscript No. _____

Please send me and bill me for

☐ no. of **reprints** via ☐ airmail (+ 25 Euro) ☐ surface mail

☐ **high-resolution PDF file** (330 Euro).

My e-mail address:

_____

Please note: It is not permitted to present the PDF file on the internet or on company homepages

★**Special Offer**★ If you order 200 or more reprints you will get a PDF file for half price.

Information regarding VAT
Please note that from German sales tax point of view, the charge for **Reprints, Issues or Posters** is considered as **"supply of goods"** and therefore, in general, such delivery is a subject to German sales tax. However,this regulation has no impact on customers located outside of the European Union. Deliveries to customers outside the Community are automatically tax-exempt. Deliveries within the Community to institutional customers outside of Germany are exempted from the German tax (VAT) only if the customer provides the supplier with his/her VAT number. The VAT number (value added tax identification number) is a tax registration number used in the countries of the European Union to identify corporate entities doing business there. It starts with a country code (e.g. FR for France, GB for Great Britain) and follows by numbers.

Cover Posters

Posters are available of all the published covers and frontispieces in two sizes

☐ DIN A2 42 x 60 cm/ 17 x 24in (one copy: **39 Euro**)

☐ DIN A1 60 x 84 cm/ 24 x 33in (one copy: **49 Euro**)

Postage for shipping posters overseas by airmail:
+ 25 Euro

Postage for shipping posters within Europe by surface mail:
+ 15 Euro

Mail reprints / cover posters to:

_____
_____
_____
_____
_____

Invoice address:

_____
_____
_____
_____
_____

Date, Signature **Stamp**

VAT no.: _____
(institutes / companies in EU countries only)

Purchase Order No.: _____

Credit Card Payment

VISA, MasterCard, AMERICAN EXPRESS
Please use the Credit Card Token Generator located at the website below to create a token for secure payment. The token will be used instead of your credit card number.

Credit Card Token Generator:
https://www.wiley-vch.de/editorial_production/index.php

Please transfer your token number to the space below.

Credit Card Token Number:

Price list for reprints (The prices include mailing and handling charges. All Wiley-VCH prices are exclusive of VAT)

No. of pages	Price (in Euro) for orders of 50 copies	100 copies	150 copies	200 copies	300 copies	500 copies
1-4	345	395	425	445	548	752
5-8	490	573	608	636	784	1077
9-12	640	739	786	824	1016	1396
13-16	780	900	958	1004	1237	1701
17-20	930	1070	1138	1196	1489	2022
for every additional 4 pages	147	169	175	188	231	315

★ **Special Offer** ★ If you order 200 or more reprints you will get a PDF file for half price.

Wiley-VCH Verlag GmbH & Co. KGaA; Location of the Company: Weinheim;
Chairman of the Supervisory Board: John Kritzmacher,
Trade Register: Mannheim, HRB 432833, General Partner: John Wiley & Sons GmbH,
Location: Weinheim, Trade Register Mannheim, HRB 432296,
Managing Directors: Sabine Steinbach, Dr. Guido F. Herrmann

WILEY-VCH